NASA Technical Paper 2503

December 1985

Compressible, Unsteady Lifting-Surface Theory for a Helicopter Rotor in Forward Flight

Harry L. Runyan
and Hsiang Tai

(NASA-TP-2503) COMPRESSIBLE, UNSTEADY LIFTING-SURFACE THEORY FOR A HELICOPTER ROTOR IN FORWARD FLIGHT (NASA) 21 p HC A02/MF A01 CSCL 01A

N86-18289

Unclas H1/02 03997

NASA

NASA Technical Paper 2503

1985

Compressible, Unsteady Lifting-Surface Theory for a Helicopter Rotor in Forward Flight

Harry L. Runyan
and Hsiang Tai

Langley Research Center
Hampton, Virginia

National Aeronautics
and Space Administration

Scientific and Technical Information Branch

Summary

A lifting-surface theory has been developed for a helicopter rotor in forward flight for compressible and incompressible flow. The method utilizes the concept of the linearized acceleration potential and makes use of the doublet lattice procedure. Calculations demonstrating the application of the method are given in terms of the lift distribution on a one-bladed rotor, a two-bladed rotor, and a rotor with swept-forward and swept-back tips. Also, the lift on a rotor vibrating in a pitching mode at 4 per revolution is given. Compressibility effects and interference effects for a two-bladed rotor are discussed.

Introduction

The aerodynamics of rotating elements, such as helicopter rotors and propellers, has been under extensive study since the advent of the airplane, and, with a combination of experimental and analytical approaches, succcessful designs have been achieved. In many cases, two-dimensional theory has been used, usually modified by assumed spanwise distribution and inflow velocities. This report presents a compressible, unsteady lifting-surface method for a helicopter rotor in forward flight within the limits of linear aerodynamic theory.

The method is based on the concept of the acceleration potential, originally formulated for three-dimensional oscillating lifting surfaces by Küssner (1941). The method was first applied to an oscillating wing in uniform rectilinear motion, including effects of compressible flow by Runyan and Woolston (1957). The acceleration-potential approach has now become standard in the determination of the unsteady aerodynamic forces for flutter studies of lifting surfaces in rectilinear motion.

An early use of the acceleration-potential approach for a rotating system was made in a paper by Hanaoka (1962) for the loading on a marine propeller in incompressible flow. The acceleration potential has been used in the past for studying the propeller noise problem. In all these noise propagation cases, the problem was specialized early in the analytical development to the so-called far-field case usually with a stationary observer. However, the lifting-surface theory is essentially concerned with the details of the near-field case for a co-moving observer and with the satisfaction of certain boundary conditions. Runyan (1973) utilized the acceleration-potential approach to obtain a solution for the oscillating propeller in compressible flow. Suciu et al. (1976) have derived an incompressible lifting-surface theory and applied it to a windmill. The procedure is based on the velocity-potential method and subdivides the integration areas into panels within which a constant pressure distribution is assumed. Dat (1973) derived a general expression for an acceleration doublet for any motion. The theory developed by Dat was applied to a helicopter in forward flight by Costes (1973). The approach of Costes is similar to the method given in this paper, with the exception of a numerical differentiation procedure which is adopted to obtain the downwash velocity from the velocity potential. In the present approach, the expression for downwash velocity is obtained analytically and includes a number of implicit differentiations. Pierce and Vaidyanathan (1983) treated the helicopter rotor in forward flight using the method of matched asymptotic expansion for the incompressible case.

The method presented in this report sets forth a formulation of fundamental, three-dimensional, compressible, unsteady aerodynamic theory for propellers and helicopter rotors in forward flight. An inertial coordinate system is adopted, and the integrations involved in solving the integral equation are formulated for arbitrary space-time variations. In this formulation, singular terms arise in the integrations and are handled by the technique of the finite-part integrals.

The paper is divided into three basic sections. The first section contains a brief derivation of the fundamental equations and is followed by a section describing a method of solving the integral equation. Finally, the method is applied to specific examples, and the computational results are given.

Symbols

A, B	coefficient in equations (28)
A'	rotor-blade area
A_{nm}	aerodynamic-influence coefficients
A_n, B_n	Fourier coefficients
C	chord of rotor
C_T	thrust coefficient (Thrust/$\pi\rho\Omega^2 R_t^4$) where thrust is normal to tip-path plane and is positive in positive z-direction
c	speed of sound
D	absolute value of $\vec{D}$
$\vec{D}$	radius vector from doublet to downwash point
$\hat{D}$	$= \vec{D}/D$, unit vector of $\vec{D}$

h	flapping deflection, positive up
h_o	magnitude of flapping deflection
I	value of singular integral
K	kernel function
L.E.	leading edge
M_{tip}	tip Mach number
ℓ, m, n	direction cosines of $\vec{n}$
ℓ_o, m_o, n_o	direction cosines of $\vec{n}_o$
$\vec{n}$	unit vector at downwash point, normal to velocity vector
$\vec{n}_o$	unit vector at doublet point, normal to velocity vector surface
p	pressure
q	source or doublet strength
R_s	rotor root radius
R_t	rotor tip radius
r	distance of downwash point along span
r_ℓ, r_u	lower and upper bounds of panel in spanwise direction
r_o	distance of doublet along span
$\hat{r}_o$	distance of doublet along span at singular point time
$\bar{r}_o$	$= (r_\ell + r_u)/2$
T.E.	trailing edge
t	field time
U	velocity of rotor system, parallel to x-axis, positive in negative x-direction
$\vec{V}$	velocity at downwash points
V_n	resultant velocity normal to blade
$\vec{V}_o$	velocity of doublet
W	velocity of rotor system, parallel to z-axis
w_n	downwash velocity, normal to velocity plane, positive down
$\vec{X}$	position vector of downwash point from inertial frame origin
$\vec{X}_o$	position vector of doublet from inertial frame origin
x, y, z	Cartesian coordinates of downwash point
x_o, y_o, z_o	Cartesian coordinates of doublet position
x_α	distance from pitch axis to downwash point
α	twist angle at downwash point as a function of t
α_o	twist angle at doublet position as a function of τ
α_r	angle of axis of rotation relative to z-axis
$\vec{\beta}$	$\vec{V}_o/c$
θ	angular position of blade at time t, $\theta = \Omega t$
θ_B	blade pitch angle relative to plane of rotation
θ_o	angular position of blade at time τ, $\theta_o = \Omega\tau$
θ_n	angle of velocity vector V_n
θ_w	blade angle of attack
μ	advance ratio, $U/\Omega R_t$
ρ	air density
τ, τ_o	source time
$\hat{\tau}$	source time at which integrand in equation (25) becomes singular
ϕ	velocity potential
ϕ_D	velocity potential of a moving doublet
ϕ_s	velocity potential for a moving source
Ψ	acceleration potential
Ψ_s	acceleration potential for a moving source
ψ	azimuth angle measured from downwind position
Ω	rotation speed of rotor
ω_h	flapping frequency
ω_α	pitching frequency

A dot over a symbol indicates derivative with respect to time.

Basic Formulation

The formulation of the aerodynamic equations is based on the linearized acceleration-potential approach. The fluid is considered perfect, with no

separation, and the formulation is based upon the assumption of small perturbations. One reason for adopting the acceleration-potential approach is that the pressure discontinuity occurs only on the surface of the blade, and thus the boundary conditions need only be applied on the blade surface, and not throughout the wake. The blade is treated as a very thin surface of discontinuity across which a pressure jump occurs. The effect of compressibility is taken into account by utilizing the complete linearized potential for a lifting doublet and by utilizing the effects of retarded time.

As shown in sketch 1, an inertial coordinate system was used. The helicopter rotor moves in the negative x-direction with velocity U, moves in the positive z-direction with velocity W, and rotates counterclockwise with a constant angular velocity Ω. A point of interest on the rotor blade is designated by the vector $\vec{X}_o(\tau)$ from the origin of the ground-based coordinate system.

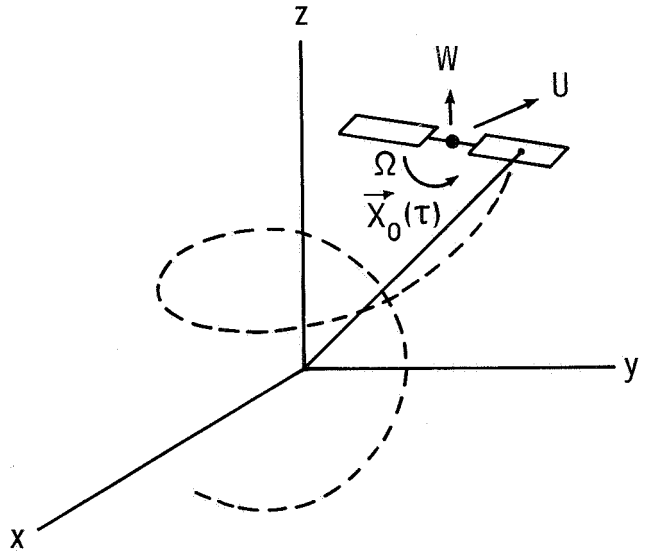

Sketch 1

If Ψ is the acceleration potential of a source (or doublet), the perturbation pressure is then given by

$$p = -\rho\Psi \tag{1}$$

This expression represents the pressure p at point $\vec{X}$ due to a single source (or doublet) located at $\vec{X}_o$. The potential Ψ contains a constant value of q, which represents the strength of the source and thus the magnitude of the pressure. In this form, there is no boundary condition available to determine the value of the arbitrary constant q and the resulting pressure. Since the spatial derivative of a velocity potential represents a velocity, it is convenient to use the relationship between the velocity potential and the acceleration potential to provide an equation for applying the boundary condition of "no flow" through the rotor surface. The relationship between the pressure and velocity potential for an inertial coordinate system is

$$p = -\rho\frac{D\phi}{Dt} \tag{2}$$

where $\frac{D\phi}{Dt}$ is the substantive derivative. Dropping out the second-order terms and integrating with respect to observer time results in

$$\phi(t) = \int_{-\infty}^{t} \Psi(t')dt' \tag{3}$$

Taking the derivative of ϕ with respect to a direction $\vec{n}$ gives the fluid velocity component in the direction $\vec{n}$ as follows:

$$\Delta w_n = \frac{\partial\phi}{\partial n} = \frac{\partial}{\partial n}\int_{-\infty}^{t} \Psi\, dt' \tag{4a}$$

The right-hand side of equation (4a) represents an induced velocity in the direction $\vec{n}$ due to a moving source (or doublet) of strength q where the value of q is contained in the expression for Ψ. By adding the contribution of all doublets distributed over the rotor, the induced velocity along $\vec{n}$ at the downwash point can be represented as

$$w_n = \int \Delta w_n\, dA' = \int \frac{\partial}{\partial n}\int_{-\infty}^{t} \Psi\, dt'\, dA' \tag{4b}$$

The left-hand side, w_n, represents the known boundary condition and is the velocity normal to the velocity vector at the downwash point. (A discussion of w_n is included in the section entitled "Definition of Boundary Conditions.") Thus, the problem resolves itself by setting up a method of solution of equation (4b) from which the values of q, the unknown, can be determined which satisfy the known velocity boundary conditions w_n. The next section contains the development of the expression for an acceleration doublet potential.

Acceleration Potential of a Doublet in Compressible Flow

The acceleration potential Ψ_s must satisfy the wave equation

$$\nabla^2\Psi_s - \frac{1}{c^2}\frac{\partial^2\Psi_s}{\partial t^2} = f(\vec{X}, t) \tag{5}$$

where $f(\vec{X},t)$ is a source distribution. Furthermore, if the path of an isolated source is a variable of a function of time $\vec{X}_o(t)$, then $f(\vec{X},t) = q\delta[\vec{X}-\vec{X}_o(t)]$, where δ is the Dirac delta function.

Using the Green's function formulation, the acceleration-potential expression for a moving source, Ψ_s can be written as (Morse and Feshbach 1978, page 841)

$$\Psi_s(\vec{X},t) = \frac{q(\vec{X}_o,\tau)}{4\pi\left|\vec{X}-\vec{X}_o(\tau)\right|\left|1-\frac{\vec{V}_o(\tau)\cdot[\vec{X}-\vec{X}_o(\tau)]}{c\left|\vec{X}-\vec{X}_o(\tau)\right|}\right|} \tag{6}$$

where $\vec{X}_o(\tau)$ designates the position of the source at time τ, $\vec{X}$ is the position of the field point at time t, $\vec{V}_o(\tau)$ is the velocity of the source point at time τ, c is the speed of sound, and q is the strength of the source. An auxiliary equation which relates the time interval $(t-\tau)$ to the distance between the two points is given as follows:

$$t-\tau = \frac{\left|\vec{X}-\vec{X}_o(\tau)\right|}{c} \tag{7}$$

and is usually referred to as the causality condition. Equation (6) expresses the potential as a function of τ, and only through equation (7) as an implicit function of t and $\vec{X}$.

From equations (3) and (6), the velocity potential due to a moving source is

$$\begin{aligned}\phi_s(t) &= \int_{-\infty}^{t}\Psi_s(t')\,dt' = \int_{-\infty}^{t}\frac{q(\tau')}{4\pi(D-\vec{D}\cdot\vec{\beta})}dt' \\ &= \frac{1}{4\pi}\int_{-\infty}^{\tau}\frac{q(\tau')}{D(\tau')}d\tau'\end{aligned} \tag{8}$$

where $\vec{D} = \vec{X}-\vec{X}_o$, $D = |\vec{D}|$, and $dt' = \left(1-\frac{\vec{D}\cdot\vec{\beta}}{D}\right)d\tau'$. The quantities τ', t', and t, τ satisfy equation (7).

A source potential cannot be used to produce a pressure difference across a lifting surface. However, a doublet does contain the proper form of the singularity on the surface to provide a jump in pressure over the lifting surface. The expression for a doublet potential can be obtained by taking the derivative of a source potential in a direction normal to the airfoil surface. If $\vec{n}_o$ designates the normal to the airfoil surface, then

$$\begin{aligned}\phi_D(t) &= \frac{\partial}{\partial n_o}\phi_s(t) = \vec{n}_o\cdot\nabla_{\vec{X}_o}\phi_s = -\vec{n}_o\cdot\nabla_{\vec{X}}\phi_s \\ &= \frac{\vec{n}_o\cdot\vec{D}q}{4\pi c(D-\vec{\beta}\cdot\vec{D})D}\bigg|_{\tau} + \int_{-\infty}^{\tau} q\frac{\vec{n}_o\cdot\vec{D}}{4\pi D^3}d\tau'\end{aligned} \tag{9}$$

Equation (9) was also derived by Dat (1973) in a different fashion. For incompressible flow, $c\to\infty$, the first term $\to 0$, and the integral remains unchanged except for the upper limit, where $\tau = t$.

To obtain the final equation for downwash Δw_n, a second directional derivative is required. This derivative is taken normal to the flight path at the location of the downwash point as follows:

$$\Delta w_n = \frac{\partial\phi_D}{\partial n} = \vec{n}\cdot\nabla_{\vec{X}}\phi_D$$

This leads to

$$\begin{aligned}\Delta w_n = \frac{q}{4\pi cD^2(1-\hat{D}\cdot\vec{\beta})}\Bigg[&(\vec{n}\cdot\vec{n}_o - \vec{n}_o\cdot\hat{D}\vec{n}\cdot\hat{D}) \\ &+ \frac{\vec{n}_o\cdot\vec{\beta}\vec{n}\cdot\hat{D} - \frac{\vec{D}}{c}\cdot\vec{\dot{n}}_o\vec{n}\cdot\hat{D} - \vec{n}_o\cdot\hat{D}\vec{n}\cdot\hat{D} + \vec{n}_o\cdot\hat{D}\vec{n}\cdot\vec{\beta}}{(1-\hat{D}\cdot\vec{\beta})} \\ &- \frac{\vec{n}_o\cdot\hat{D}\vec{n}\cdot\hat{D}\left(1-\beta^2+\frac{\vec{D}}{c}\cdot\vec{\dot{\beta}}\right)}{(1-\hat{D}\cdot\vec{\beta})^2}\Bigg]\Bigg|_{\tau_o} - \frac{\vec{n}_o\cdot\hat{D}\vec{n}\cdot\hat{D}\dot{q}}{4\pi c^2D(1-\hat{D}\cdot\vec{\beta})^2}\Bigg|_{\tau_o} \\ &+ \frac{1}{4\pi}\int_{-\infty}^{\tau_o(r_o)} q\left(\frac{\vec{n}\cdot\vec{n}_o - 3\vec{n}_o\cdot\hat{D}\vec{n}\cdot\hat{D}}{D^3}\right)d\tau\end{aligned} \tag{10}$$

This concludes the derivation of the basic equation for the downwash Δw_n at a field point created by an arbitrarily moving doublet. The term containing $\dot{q}$ in the present application was not used in subsequent calculations, since the rate of change of the loading is relatively small. Consequently, this term compared with the other terms in the brackets is relatively small. It can be argued that the ratio of the $\dot{q}$ term to the fifth term in the first bracket is $\Omega D/c$, which is small unless the frequency Ω is very large, which may be the case in other applications, such as acoustics. The remaining portion of this paper is directed towards specializing this equation for a helicopter blade moving with a forward velocity U, and a vertical velocity W, and rotating with an angular velocity Ω.

Equation (10) gives the downwash at a field point (x,y,z,t) due to a doublet placed at a point (x_o,y_o,z_o,τ) with a strength q. To form a lifting surface such as a rotor, it is necessary to distribute the doublets over the lifting surface and integrate over the surface to obtain the downwash at a field point. If the downwash is known, the quantity q can then be determined. Letting K be the expression on the right-hand side of equation (10), the final equation is

$$w_n = \iint_{A'} K\,dA' \tag{11}$$

where A' is the area of the rotor surface. This equation represents a rather formidable computing task, and the history of lifting-surface theory, even for nonrotating wings, has centered on devising approximate methods to accomplish the integration in an economical manner. One method, termed the doublet lattice method, has been very successful when applied to aircraft wings and is probably the most economical procedure of the many variants. This method was first demonstrated for the unsteady case by Runyan and Woolston (1957) and was later expanded by Albano and Rodden (1969). This is the method adopted in this paper, and the application is discussed subsequently. In the next section, the coordinate system is specified, and the doublets and downwash points are appropriately located for a helicopter rotor in forward flight.

Specification of Coordinate System

The blade has the chord C and length $R_t - R_s$, where R_s is the radial distance to the root of the blade and R_t is the distance to the tip of the blade. Sketch 2 shows the blade momentarily coinciding with the coordinate system along the positive x-axis at $t = 0$ and at a new location at time t later. The blade executes a counterclockwise rotation

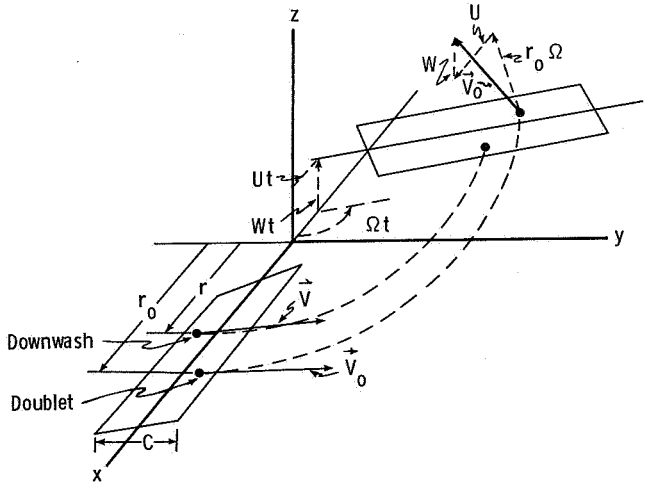

Sketch 2

with angular velocity Ω while moving with velocity U along the negative x-direction and velocity W along the positive z-direction. Since the doublet lattice method has been adopted, the doublet point for one chordwise panel lies 1/4 C ahead of the midchord, and the downwash point lies 1/4 C aft of the midchord. The positions of the doublet point and downwash point can be established as follows. The Cartesian components of the doublet position are

$$\left.\begin{aligned} x_o &= -U\tau + r_o\cos(\Omega\tau) - (C/4)\sin(\Omega\tau)\cos\alpha_o \\ y_o &= r_o\sin(\Omega\tau) + (C/4)\cos(\Omega\tau)\cos\alpha_o \\ z_o &= W\tau + (C/4)\sin\alpha_o \end{aligned}\right\} \quad (12)$$

where r_o is the radial distance of the doublet along the span. (See sketch 1.) With the substitution of $C \to -C, r_o \to r$, and $\tau \to t$, the position of the downwash point is given by

$$\left.\begin{aligned} x &= -Ut + r\cos(\Omega t) + (C/4)\sin(\Omega t)\cos\alpha \\ y &= r\sin(\Omega t) - (C/4)\cos(\Omega t)\cos\alpha \\ z &= Wt - (C/4)\sin\alpha \end{aligned}\right\} \quad (13)$$

In equations (12) and (13), the angles α and α_o are the twist angles of the velocity vectors $\vec{V}$ and $\vec{V}_o$, respectively, defined by

$$\left.\begin{aligned} \tan\alpha &= \frac{W}{U\sin(\Omega t) + r\Omega} \\ \tan\alpha_o &= \frac{W}{U\sin(\Omega\tau) + r_o\Omega} \end{aligned}\right\} \quad (14)$$

The reference plane defined by the doublets and downwash points is a twisted surface. The doublet velocity, namely the time derivative of the position vectors, can be computed from equation (12) as follows:

$$\vec{V}_o = \dot{x}_o\vec{i} + \dot{y}_o\vec{j} + \dot{z}_o\vec{k}$$

The unit vector $\vec{n}_o$ is chosen to be perpendicular to the twisted surface (see sketch 3) created by the velocity $\vec{V}_o$, which is a function of r_o (see eqs. (12) and (14)). To determine $\vec{n}_o$ as a function of τ, write

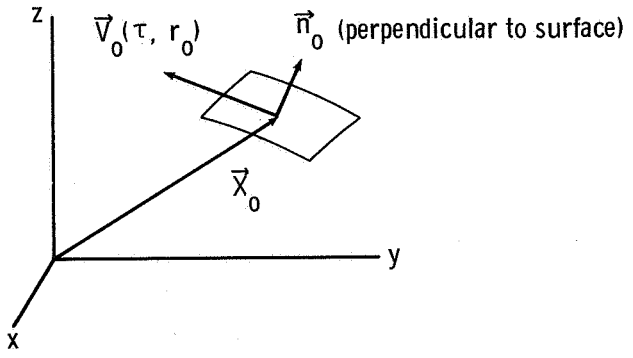

Sketch 3

$\vec{V}_o = \vec{V}_o' + W\vec{k}$, where $\vec{V}_o'$ is the projection of the doublet velocity on the horizontal plane. Then,

$$\vec{n}_o = \ell_o\vec{i} + m_o\vec{j} + n_o\vec{k} \quad (15)$$

where ℓ_o, m_o, and n_o are the directional cosines of the unit vector $\vec{n}_o$. Form the vector quantity $\vec{S}$ by making $\vec{S} = \vec{V}_o' \times W\vec{k}$. Therefore,

$$\vec{S} = W[U + r_o\Omega\sin(\Omega\tau) + (C/4)\Omega\cos(\Omega\tau)\cos\alpha_o]\vec{j} + W[r_o\Omega\cos(\Omega\tau) - (C\Omega/4)\sin(\Omega\tau)\cos\alpha]\vec{i} \quad (16)$$

Furthermore, ℓ_o, m_o, and n_o can be obtained by imposing the following conditions:

$$\left.\begin{aligned} &\vec{n}_o \perp \vec{S} \\ &\vec{n}_o \perp \vec{V}_o \\ &|\vec{n}_o| = 1 \end{aligned}\right\} \quad (17)$$

From equations (15), (16), and (17),

$$\left.\begin{aligned} \ell_o &= \frac{W[U + r_o\Omega\sin(\Omega\tau) + (C/4)\Omega\cos(\Omega\tau)\cos\alpha_o]}{V_o'\sqrt{W^2 + V_o'^2}} \\ m_o &= -\frac{W[r_o\Omega\cos(\Omega\tau) - (C/4)\Omega\sin(\Omega\tau)\cos\alpha_o]}{V_o'\sqrt{W^2 + V_o'^2}} \\ n_o &= \frac{V_o'}{\sqrt{W^2 + V_o'^2}} \end{aligned}\right\} \quad (18)$$

where V_o' is the magnitude of $\vec{V}_o'$, and

$$V_o'^2 = [U + r_o\Omega\sin(\Omega\tau) + (C/4)\Omega\cos(\Omega\tau)\cos\alpha_o]^2 + [r_o\Omega\cos(\Omega\tau) - (C/4)\Omega\sin(\Omega\tau)\cos\alpha_o]^2 \quad (19)$$

By the same procedure, $\vec{n}$ is derived by making the appropriate substitutions, $C \to -C, \alpha_o \to \alpha, \tau \to t$, etc. (i.e., $\vec{n} = \ell\vec{i} + m\vec{j} + n\vec{k}$), to get

$$\left.\begin{aligned} \ell &= \frac{W[U + r\Omega\sin(\Omega t) - (C/4)\Omega\cos(\Omega t)\cos\alpha]}{V_o'\sqrt{W^2 + V^2}} \\ m &= \frac{-W[r\Omega\cos(\Omega t) + (C/4)\Omega\sin(\Omega t)\cos\alpha]}{V_o'\sqrt{W^2 + V_o'^4}} \\ n &= \frac{V'}{\sqrt{W^2 + V'^2}} \end{aligned}\right\} \quad (20)$$

where

$$V'^2 = [U + r\Omega\sin(\Omega t) - (C/4)\Omega\cos(\Omega t)\cos\alpha]^2 + [r\Omega\cos(\Omega t) + (C/4)\Omega\sin(\Omega t)\cos\alpha]^2$$

The vector $\vec{D} = \vec{X} - \vec{X}_o$ defined in equation (8) can be expressed as

$$D = \Big(\{U(t-\tau) + r\cos(\Omega t) - r_o\cos(\Omega\tau) + (C/4)[\sin(\Omega t)\cos\alpha + \sin(\Omega\tau)\cos\alpha_o]\}^2 + \{r\sin(\Omega t) - \sin(\Omega\tau) - (C/4)[\cos(\Omega t)\cos\alpha + \cos(\Omega\tau)\cos\alpha_o]\}^2 + [W(t-\tau) - (C/4)(\sin\alpha_o + \sin\alpha)]^2\Big)^{1/2} \quad (21)$$

With the substitution of the quantities $\vec{n}_o, \vec{n}, \vec{V}_o, \vec{V}, \vec{D}$, and D into equation (11), the integral equation was solved for the unknown $q(r_o, \tau)$ by using a collocation process based on the doublet lattice assumption. The kernel is singular when $D = 0$, and this was handled by use of the finite-part technique.

Solution of Integral Equation

The basic integral equation to be solved (eq. (11)) is

$$w_n = \iint_{A'} K\, dA'$$

This equation states that doublets of strength q are distributed over the area of the rotor surface A', and the induced velocity normal to the blade surface is equated to the normal velocity of the blade, where w_n is the boundary condition on the blade surface and is a known quantity. Thus, the only unknown in the integral equation is the strength of the doublet q. As mentioned previously, one method for obtaining a solution to this equation is termed the doublet lattice method and is used in this report. It has been used successfully for the wing in pure translational motion. One of the advantages of the doublet lattice method is that it eliminates the chordwise integration and thus reduces computing costs. The reduction is the result of a judicious choice of the location of the doublet and the downwash points.

Doublet Lattice Technique

In following the doublet lattice technique, the rotor is divided into a number of panels, both spanwise and chordwise. In each panel, a line of doublets of unknown strength q_i is located at the 25-percent chordwise location of the particular panel, and the downwash is evaluated at the 75-percent chordwise location and midspan of the panel (see sketch 4) for a rotor divided into 2 chordwise panels. The problem is then resolved by performing an integration from r_ℓ to r_u for the vortex at $C/8$ for the downwash point in the middle of the spanwise panel at $3C/8$ ($w_n = w_1$). The effect of the same vortex must be determined for the downwash located at $7C/8$ ($w_n = w_2$). A similar calculation is made for all the remaining vortices, including lateral distances. Therefore, a collocation procedure is used to obtain a set of equations in terms of the unknown loadings q_i.

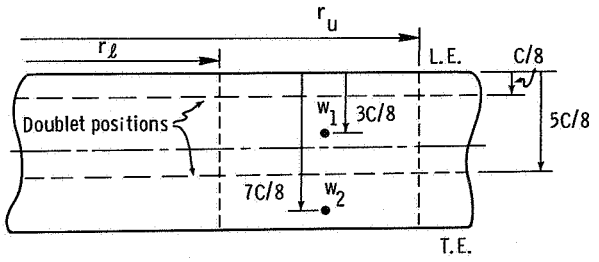

Sketch 4

The term $q(r_o, \tau)$ represents the strength of the doublet located at r_o and at time τ, and is proportional to the unknown loading. Within a particular panel, q is assumed to be constant in the spanwise direction. To account for unsteadiness, a solution was formulated to take into account the time variation of the strength of the doublet. The time variation of q is represented by assuming a Fourier series of the form

$$q(r_o, \tau) = A_o(r_o) + \sum_{n=1}^{m} [A_n(r_o)\cos(n\Omega\tau) + B_n(r_o)\sin(n\Omega\tau)] \tag{22}$$

If $q(r_o, \tau)$ is assumed to be a function of r_o alone, which means that the doublet strength does not vary with time, the Fourier series reduces to $q(r_o) = A_o$. A solution obtained with this approximation is termed the quasi-steady solution.

This series (eq. (22)) was inserted into the basic equation (eq. (11)) and integrated with respect to τ. However, there were more unknowns than simultaneous equations to solve for the unknowns. The additional required equations were obtained by evaluating equation (11) at a number of azimuth locations. For instance, if $m = 1$, then

$$q(r_o, \tau) = A_o + A_1\cos(\Omega\tau) + B_1\sin(\Omega\tau) \tag{23}$$

The azimuth was divided into equal segments of 120°, and the proper boundary conditions were applied at $\psi = 0°, 120°$, and 240°. Thus, the necessary additional equations were provided.

A set of equations is obtained as shown below:

$$\left.\begin{aligned} w_1 &= A_{11}q_1 + A_{12}q_2 + \cdots + A_{1m}q_m \\ w_2 &= A_{21}q_1 + A_{22}q_2 + \cdots + A_{2m}q_m \\ &\vdots \\ w_n &= A_{n1}q_1 + A_{n2}q_2 + \cdots + A_{nm}q_m \end{aligned}\right\} \tag{24}$$

where $A_{nm} = \int_{r_\ell}^{r_u} K_{nm}\, dr_o$ and where n refers to the downwash point and m refers to the panel number.

The rotor can be divided into any number of segments both chordwise and spanwise, with more segments resulting in more accurate results. However, the computing time and costs increase rapidly (roughly proportional to the square of the numbers of segments) as the number of segments is increased; therefore, a balance must be considered in any given situation, and there must be a trade-off between computing costs and desired accuracy.

Numerical Integration of Kernel

A closed-form integration of the kernel has not been found; therefore, the integration was performed by numerical integration, except for the area surrounding the singularity. The integration domain was divided into five areas. (See sketch 5.) The integral over areas 1 to 4 (hatched) were computed numerically by using the two-dimensional Romberg quadrature (Davis and Rabinowitz, 1984) and the contribution of the singular region (unhatched) was obtained in closed form by consideration of the finite part, as shown in the next section.

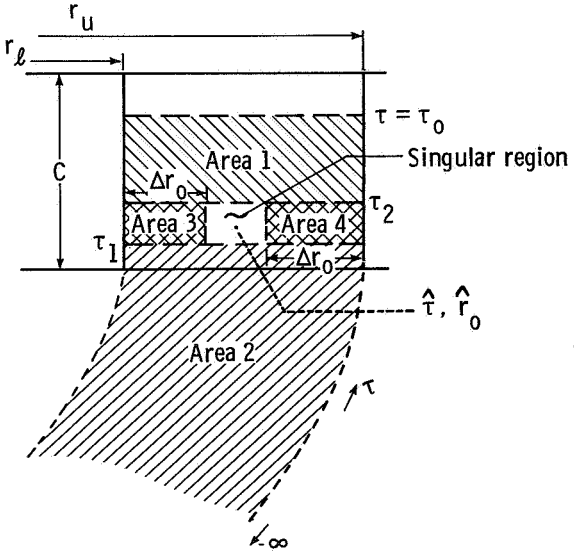

Sketch 5

The integral in the downwash equation (eq. (10)), is singular when $D \to 0$ and produces a complication which must be properly treated. The integration along τ is the path the doublet has taken in arriving at the final doublet point at $(C/4, r_o)$ measured in the local blade coordinates. The integration takes place along the path from $\tau = -\infty$ to the final doublet position at τ_o. The distance D is the distance from the integration point at time τ to the downwash point at $\vec{X}$.

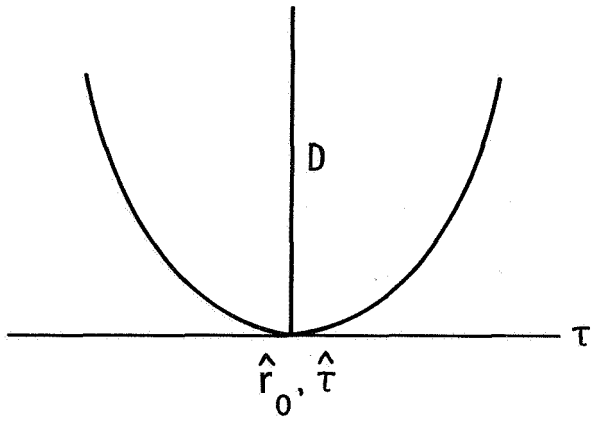

Sketch 6

There is a particular set of values of r_o and τ for which the denominator D approaches zero, and the result is an infinite integrand. The function is given above in sketch 6. The singular part of the kernel is

$$I = \int_{r_\ell}^{r_u} \int_{\tau_1}^{\tau_2} \frac{\vec{n} \cdot \vec{n}_o - 3(\hat{D} \cdot \vec{n})(\hat{D} \cdot \vec{n}_o)}{D^3} d\tau_o \, dr_o \quad (25)$$

As $D \to 0$ at the downwash point, $\hat{D}$ becomes perpendicular to $\vec{n}$; therefore, at the singular point, the second term is zero and is neglected in the treatment of the singularity. However, this second term is retained in all the numerical integrations involving areas 1 to 4 because it represents an important interference term, particularly when the blade is passing over a trailing wake. The time and distance at which I becomes singular are designated by $\hat{\tau}$ and $\hat{r}_o$. The domain of the integration in equation (25) consists of a rectangle in which the duration $\tau_2 - \tau_1$ is kept extremely small. In other words, the integration is performed along a slit in r_o, over which the second term in equation (25) is negligible. Therefore, the integral I can be approximated by

$$I = \int_{r_\ell}^{r_u} \int_{\tau_1}^{\tau_2} \frac{\vec{n} \cdot \vec{n}_o}{D^3} d\tau dr_o \quad (26)$$

By squaring the quantities in D (eq. (21)) and collecting coefficients of r_o, the distance D can be written as

$$D = (r_o^2 - 2Br_o + A)^{1/2} \quad (27)$$

where

$$B = \cos\theta_o[U(t-\tau) + r\cos\theta + C/4(\sin\theta\cos\alpha + \sin\theta_o\cos\alpha_o)] + \sin\theta_o[r\sin\theta - C/4(\cos\theta\cos\alpha + \cos\theta_o\cos\alpha_o)] \quad (28a)$$

$$A = [U(t-\tau) + r\cos\theta + C/4(\sin\theta\cos\alpha + \sin\theta_o\cos\alpha_o)]^2 + [r\sin\theta - C/4(\cos\theta\cos\alpha + \cos\theta_o\cos\alpha_o)]^2 + [W(t-\tau) - C/4(\sin\alpha + \sin\alpha_o)]^2 \quad (28b)$$

In this equation, α_o, defined in equation (14), is a function of r_o. By using the doublet lattice method, the rotor is divided into spanwise segments from r_ℓ to r_u. If these segments are small, α_o will vary approximately as

$$\frac{d\alpha_o}{dr_o} \approx -\frac{W\Omega}{(U\sin\theta_o + r_o\Omega)^2 + W^2} \quad (29)$$

If the value of α_o is approximated as a constant and evaluated at midsegment $\bar{r}_o$, it is possible to integrate equation (26) in closed form in the r_o direction. This is quite acceptable in the helicopter mode. That is, both α_o and $d\alpha_o/dr_o$ are small. Therefore, reversing the order of integration gives

$$I = \int_{\tau_1}^{\tau_2} \int_{r_\ell}^{r_u} \frac{\vec{n} \cdot \vec{n}_o}{(r_o^2 - 2Br_o + A)^{3/2}} dr_o \, d\tau \quad (30)$$

The vector $\vec{n}_o$ is also a function of r_o, but in the region of the singularity it has a very small variation and is evaluated at the singular position $(\hat{\tau}, \hat{r}_o)$. Performing the r_o integration results in

$$I = \int_{\tau_1}^{\tau_2} \frac{\vec{n} \cdot \vec{n}_o}{A - B^2} \left(\frac{r_u + B/2}{\sqrt{r_u^2 - 2Br_u + A}} - \frac{r_\ell + B/2}{\sqrt{r_{\ell 2} + 2Br_\ell + A}} \right) d\tau_o \quad (31)$$

The singular term in this expression is $A - B^2$.

Equation (31) may also be written as

$$I = \int_{\tau_1}^{\tau_2} \frac{g(\tau)}{f(\tau)} d\tau$$

where $f(\tau)$ is the singular part and $f(\tau) = A - B^2$ and $g(\tau)$ is the nonsingular part as follows:

$$f(\tau) = \left(U(t-\tau) - r\sin[\Omega(t-\tau)] + C/4\{\cos[\Omega(t-\tau)]\cos\alpha + \cos\alpha_o\}\right)^2 + [W(t-\tau) - C/4\sin\alpha + \sin\alpha_o]^2 \quad (32)$$

Equation (32) shows that $f(\tau)$ is nonnegative, so the zero of $f(\tau)$, at $\tau = \hat{\tau}$, is a second-order zero.

Expanding $f(\tau)$ in a Taylor series about the singular point $\hat{\tau}$ yields

$$f(\tau) = f(\hat{\tau}) + f'(\hat{\tau})(\tau - \hat{\tau}) + f''(\hat{\tau})(\tau - \hat{\tau})^2/2 + \cdots \quad (33)$$

Since $f(\hat{\tau})$ is a second-order zero,

$$f(\hat{\tau}) = f'(\hat{\tau}) = 0 \tag{34}$$

The conditions given by equation (34) have been verified numerically. If only the square term is kept in equation (33), equation (31) can be written as

$$I = \int_{\tau_1}^{\tau_2} \frac{2}{f''(\hat{\tau})} \left[\frac{g(\hat{\tau})}{(\tau - \hat{\tau})^2} + \frac{g'(\hat{\tau})}{(\tau - \hat{\tau})} + \frac{g''(\hat{\tau})}{2} \right] d\tau \tag{35}$$

In equation (35), if τ_2 and τ_1 are chosen symmetrically about $\hat{\tau}$, the odd derivative terms integrate to zero. Futhermore, the third term can be neglected, since $g''(\hat{\tau})$ is small. The major contribution comes from the first term. Then, using the standard integration technique (Mangler 1951), the final result for the integral is

$$I = -\frac{g(\hat{\tau})}{f''(\hat{\tau})} \frac{4}{\Delta\tau} \tag{36}$$

where $2\Delta\tau = \tau_2 - \tau_1$, and $\tau_1 < \hat{\tau} < \tau_2$.

A numerical problem arises, because this finite-part integration results in a negative number close to the total of the surrounding numerical integration areas, which are positive. Thus, it is necessary to take the difference between large numbers, and the final integration accuracy is dependent on the accuracy of the two integrations. On the one hand, the numerical integration is more accurate if $\Delta\tau$ is kept large, because the very large values of the integrand near the singularity are avoided. On the other hand, regarding the finite-part integration, the denominator was expanded in a Taylor series about the singular point $\hat{\tau}$. Therefore, it is desirable to maintain $\Delta\tau$ as small as possible to keep within the limits of the applicability of the series expansion. Numerous calculations were made, varying $\Delta\tau$ until a reasonable convergence was found. The value used for the calculations in this report was $0.01(t - \hat{\tau})$, or 1 percent of the time difference. Actually, there is little difference between 1 percent or 10 percent of the time difference, and the computing time and cost are considerably reduced by using 10 percent. For trend studies 10 percent is recommended principally to reduce computer costs. However, for final-design-type analysis, 1 percent is recommended.

For the spanwise direction, Δr_o is also an integration-limit variable. The finite-part integral was obtained by approximating the angle of twist of the velocity vector across a segment. This approximation is made by assuming that the angle of twist is constant across the segment, with a value determined at the center of segment. Numerical experimentation indicates that for a helicopter, $\Delta r_o = 0$ is satisfactory.

Definition of Boundary Conditions

The integral equation (eq. (11)) equates the induced velocity caused by a distribution of doublets (right-hand side) to the velocity normal to the velocity vector (left-hand side) to form the boundary condition of no flow through the blade. The preceding sections have shown the development of the aerodynamic induced velocity in terms of the unknown loadings q_i. This section contains a definition of w_n for several conditions.

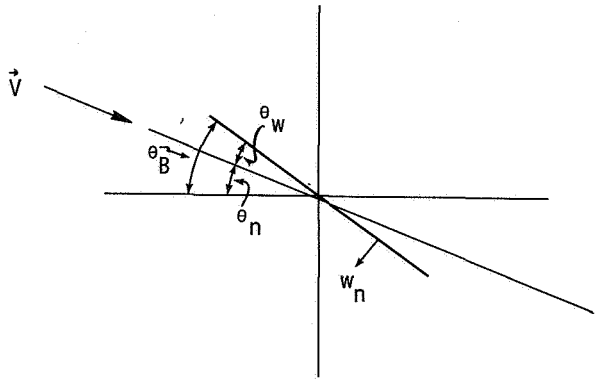

Sketch 7

Sketch 7 illustrates the geometric condition at a particular azimuth ψ and radial distance r on the blade. The angle θ_B represents the physical angle of the blade relative to the x-y plane. The angle θ_n represents the angle of the velocity vector V_n normal to the centerline of the blade. The angle θ_w is the blade angle of attack; therefore,

$$\theta_w = \theta_B - \theta_n \tag{37}$$

where

$$\theta_n = \tan^{-1} \frac{W}{(r\Omega + U \sin \Omega t)} \tag{38}$$

The velocity normal to the velocity vector V_n is

$$w_{n,o} = V_n \tan \theta_w \tag{39}$$

where

$$V_n = \sqrt{(r\Omega + U \sin \Omega t)^2 + W^2}$$

If the blade has a built-in twist, then θ_B is a function of r and would be calculated at the appropriate downwash points.

For a rotor having a swash plate,

$$\theta_s = A_o - A_1 \cos(\Omega t) - B_1 \sin(\Omega t) - A_2 \cos(2\Omega t) - B_2 \sin(2\Omega t) + \cdots \tag{40}$$

An additional contribution to the normal velocity results from the rate of pitching of the blade. If the distance from the pitch axis to the downwash point is denoted by x_α, the normal velocity to be added is

$$w_{n,s} = x_\alpha \dot{\theta}_s \tag{41}$$

For a wing harmonically vibrating in a pitching mode defined by θ_α,

$$\theta_B = \theta_\alpha \cos(\omega_\alpha t + \phi_\alpha) \tag{42}$$

where θ_α is the deflection mode shape and is a function of r, ω_α is the frequency of pitching oscillations, and ϕ_α is the phase angle relative to $\Psi = 0$. The additional velocity to be added to w_n is

$$w_{n,\alpha} = x_\alpha \dot{\theta}_B \tag{43}$$

For a rotor oscillating harmonically in a flapping mode given by

$$h = h_o \cos(\omega_h t + \phi_n) \tag{44}$$

where h_o is the magnitude of the spanwise flapping deflection, which is a function of r, where ω_h is the flapping frequency, and where ϕ_h is the phase angle relative to $\Psi = 0$,

$$w_{n,h} = \dot{h} \tag{45}$$

Therefore, for a rotor having a swash plate defined by equation (40), vibrating in a pitching mode (eq. (42)), and vibrating in a flapping and pitching mode (eq. (44)), the final downwash equation would be

$$w_n = w_{n,o} + w_{n,s} + w_{n,\alpha} + w_{n,h} \tag{46}$$

Also, the entry of the rotor into a gust field could be handled or a propeller rotating close to the fuselage could be treated if the velocity field through which the rotating surface were known.

Application to Specific Examples

The foregoing analysis has been applied to several specific examples. (See fig. 1.) The following section presents results for several paneling configurations (e.g., 5 spanwise panels and 1 chordwise panel, designated (5-1) and 7 spanwise panels and 3 chordwise panels, designated (7-3)). The untwisted rotor blade was maintained at a constant pitch setting θ_B of 0.1 rad for all the calculations. Although the spacing of the paneling can be arbitrary, the paneling arrangements used in all examples in this paper are uniform except for the swept-tip cases, for which the arrangements are described.

Incompressible Flow

Single blade. To investigate the convergence of the method of this report when using the doublet lattice procedure, the program was run for several chordwise and spanwise elements for the incompressible case. The thrust coefficient C_T is plotted against the azimuth angle in figure 2. (In all the plots for thrust coefficient versus azimuth angle, the thrust was calculated for 16 uniformly spaced azimuth angles, and each curve was faired using a cubic spline.) The rotor was first divided into 5 spanwise panels and one chordwise panel (5-1), and the results are shown by the solid line. The chordwise division was increased to (5-2), and the results are shown by the long dashed line. It can be seen that very little change occurred. The spanwise divisions were increased to (7-1), and the largest change between various panelings occurred at $\psi = 0°$, where the difference in C_T is about 11 percent. Increasing the chordwise divisions to 3 (7-3) produced little change from the (7-1) case.

An interesting phenomenon occurs in the rotor first quadrant. For $\psi = 0$ to 37°, the lift increases to a local maximum at $\psi = 37°$, abruptly falls to a local minimum for $\psi = 60°$, and then rapidly increases to a maximum at $\psi = 100°$. A similar phenomenon is shown analytically by Egolf and Landgrebe (1983) in figure 60 of that report, where a local minimum and a local maximum occur in the same range of azimuth angles, even though the geometry of the two blades and the flight conditions are different. In figure 93 of the same report, some test data show a similar variation of loading in the same azimuth range.

The chordwise pressure distributions for the (7-3) case are presented in figure 3. In using the doublet lattice method, the loading is concentrated at the location of the doublet which for the (7-3) case is located at $0.0833C$, $0.416C$, and $0.75C$. The pressure was faired using a cubic spline through the three vortex locations and the known value of zero at the trailing edge. The distributions are given for 7 spanwise positions. In general, the curves exhibit the expected shape, with the largest values occurring as the leading edge is approached. For the span distribution, the values at $r/R_t = 0.85$ are slightly larger than the values at $r/R_t = 0.95$. These values indicate a falling off in the tip region.

From these concentrated forces, the section pitching moment can be calculated. Figure 4 presents these results for $\psi = 90°$. The section moment was taken about the 1/4 C and a nose-down moment is

taken as positive. The pitching moment shows some rather dramatic changes along the span. The moment is nose-up near the tip ($r/R_t = 0.95$), changes to a small nose-down value, then becomes nose-up for most of the inboard region. Integration of the moment would result in a total root-end pitching moment up at $\psi = 90°$.

Swept tip. The segments used for the doublet lattice for the swept tip studies were (5-1), where two equal segments were used in the tip region and three equal segments were used in the unswept inboard section. Lift is plotted against azimuth in figure 5 for the two sweep conditions and for zero sweep. In general, the three results show little difference. The swept-back configuration has the largest lift from $\psi \approx 300°$ to $40°$. For $\psi \approx 100°$ to $240°$, the swept-forward configuration has a slightly larger lift than the other configurations. The total lift for one rotation for the swept-back case and the swept-forward case appear to give about the same lift as produced by the unswept rotor. In figure 6, the lift distribution along the rotor span is given for $\psi = 0°$. The major effect of sweep is concentrated at the tip, where the swept-back tip load is greater than either the unswept or swept-forward cases. In contrast, figure 7 shows a larger forward tip load than for the unswept or swept-back tip for $\psi = 180°$.

Blade oscillating in pitch. An example of unsteady loads on a rotor blade with (5-1) paneling oscillating in a pitching mode about the midchord at a frequency of 4 per revolution (120 cycles/sec) is given in figure 8. For this case, a 17-term Fourier series ($m = 8$) was used to simulate the oscillating load, which was comprised of one constant term, 8 cosine terms, and 8 sine terms. The nonoscillating and oscillating rotor-blade loading is given for one revolution. The blade was oscillated through an angle of ± 0.1 rad about a mean angle of 0.1 rad. The effect of the oscillation is readily apparent when compared with the nonoscillatory case. With the harmonic representation of the loading, the magnitude and phase of the several harmonic loads are easily determined. The magnitudes are plotted in figure 9. The only harmonic loads that were significantly changed from the steady case were the 3rd, 4th, and 5th. All three harmonics were increased, but the 4th harmonic was drastically increased. Another calculation was made for the nonoscillating case and was compared with the quasi-steady case. Virtually no difference was observed; this similarity indicates that, at least for this case, the rate of change of loading in a revolution of the blade is small enough that the effect of a variable wake is negligible.

Compressible Flow

One-blade rotor. For a one-bladed rotor (5-1), the effect of compressibility is illustrated in figure 10, in which C_T is plotted against azimuth angle. The incompressible result is included for comparison. As expected, the compressible load is larger than the incompressible load throughout one revolution and effect is greatest in the region of the advancing blade and smallest in the retreating region.

Two-bladed rotor. The method has been extended to the two-bladed rotor (5-1 per blade) for the compressible case, and the results are shown in figure 11. The thrust coefficient C_T per blade is plotted against azimuth angle for a one-bladed rotor and for a two-bladed rotor. For azimuth angles from $\psi = 20°$ to $120°$, the one-bladed rotor has a larger C_T. For $\psi = 120°$ to $260°$, C_T on the one- and two-bladed rotors are approximately the same. However, for $\psi = 260°$ to $340°$, a drastic reduction in lift per blade occurs for the two-bladed rotor compared with the results for the one-bladed rotor. The lowest lift occurs at $\psi = 292°$; this places the other blade of the two-bladed rotor at $\psi = 112°$, the point of maximum lift. Apparently, the high lift on the blade at $\psi = 112°$ creates a very unfavorable induced velocity on the second blade at $\psi = 292°$, which requires the loading to go to zero to satisfy the boundary conditions at $\psi = 292°$.

Concluding Remarks

A linearized lifting-surface theory, including the effects of compressibility, has been developed for a helicopter rotor in forward flight. The method utilizes the concept of the acceleration potential and makes use of the doublet lattice procedure for performing the required integrations. Also, the method has been extended to include the effects of unsteady flow and blade motion.

Sample calculations have been done for several cases. These include the effect of swept-back and swept-forward tips. The effect of these two tip configurations was minimal on the total loading for one revolution. However, the loading distribution changed considerably for several azimuth positions ψ. Compressibility was investigated for one configuration. As expected, the effect was greatest in the advancing-blade region ($\psi = 90°$) and was minimal in the retreating-blade region. A comparison of the thrust coefficient C_T of a one-bladed rotor and a two-bladed rotor was made. In the azimuthal range between $20°$ and $120°$, the one-bladed rotor showed higher lift. However, between $\psi = 260°$ and $340°$, the two-bladed rotor showed lower C_T. The effect on C_T of

a blade oscillating in pitch at 4 per revolution has been shown. The effect on the total blade lift has been shown and the effect of the oscillation is readily apparent. The harmonic content was calculated, and the greatest difference between the oscillatory and nonoscillatory cases was in the 4th harmonic.

NASA Langley Research Center
Hampton, VA 23665-5225
September 3, 1985

References

Albano, Edward; and Rodden, William P. 1969: A Doublet-Lattice Method for Calculating Lift Distributions on Oscillating Surfaces in Subsonic Flows. *AIAA J.*, vol. 7, no. 2, Feb., pp. 279–285; Errata, vol. 7, no. 11, Nov., p. 2192.

Costes, J.-J. 1973: *Computation of Unsteady Aerodynamic Forces on Helicopter Rotor Blades.* NASA TT F-15,039.

Dat, Rolland 1973: *La Théorie de la Surface Portante Appliquée a l'Aile Fixe et a l'Hélice (The Lifting Surface Theory Applied to Fixed Wings and Propellers).* ONERA T.P. No. 1298.

Davis, Phillip F.; and Rabinowitz, Philip 1984: *Methods of Numerical Integration*, Second ed. Academic Press, Inc.

Egolf, T. Alan; and Landgrebe, Anton J. 1983: *Helicopter Rotor Wake Geometry and Its Influence in Forward Flight. Volume I—Generalized Wake Geometry and Wake Effect on Rotor Airloads and Performance.* NASA CR-3726.

Hanaoka, T. 1962: Hydrodynamics of an Oscillating Screw Propeller. *Fourth Symposium on Naval Hydrodynamics—Propulsion Hydroelasticity*, Office of Naval Research, pp. 79–124.

Küssner, H. G. 1941: *General Airfoil Theory.* NACA TM 979.

Mangler, K. W. 1951: *Improper Integrals in Theoretical Aerodynamics.* Rep. No. Aero. 2424, British R.A.E., June.

Morse, Phillip M.; and Feshbach, Herman 1978: *Methods of Theoretical Physics.* McGraw-Hill Book Co., Inc.

Pierce, G. Alvin; and Vaidyanathan, Anand R. 1983: *Helicopter Rotor Loads Using Discretized Matched Asymptotic Expansions.* NASA CR-166092.

Runyan, Harry Laird, Jr. 1973: Unsteady Lifting Surface Theory Applied to a Propeller and Helicopter Rotor. Ph.D. Thesis, Loughborough, Univ. of Technol., July.

Runyan, Harry L.; and Woolston, Donald S. 1957: *Method for Calculating the Aerodynamic Loading on an Oscillating Finite Wing in Subsonic and Sonic Flow.* NACA Rep. 1322. (Supersedes NACA TN 3694.)

Suciu, Emil O.; Preuss, Robert; and Morino, Luigi [1976]: *Computational Aerodynamic Analysis of Horizontal-Axis Windmills.* ENGR-CCMP-TR-76-01 (NSF Grant No. AER-75-00548), College of Engineering, Boston Univ.

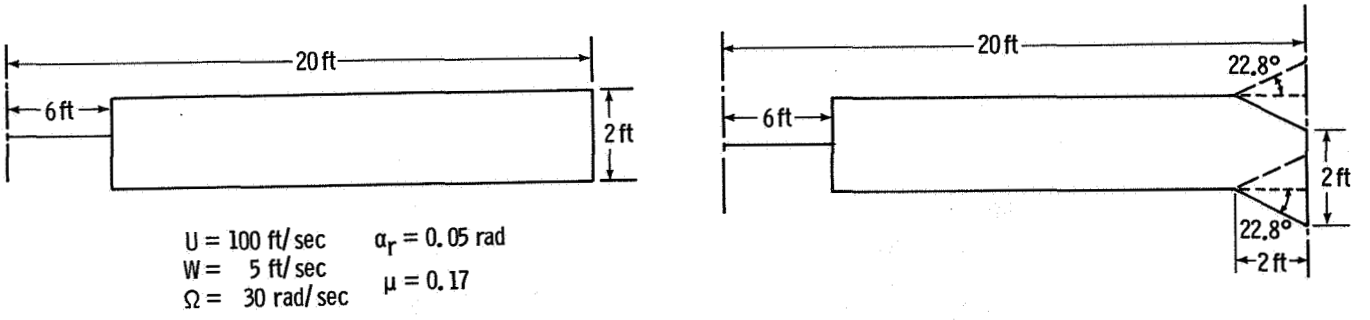

Figure 1. Configurations used in examples and input parameters.

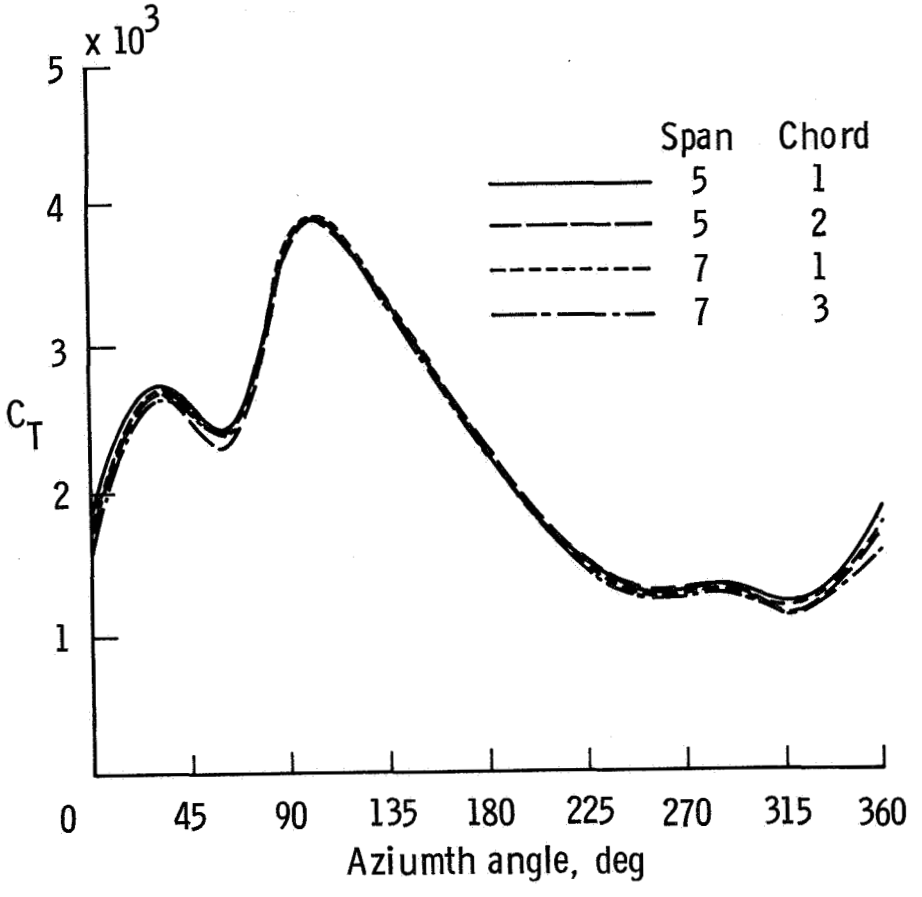

Figure 2. Four panel configurations for a single rotor blade. Incompressible; $\mu = 0.17$; $\theta_B = 0.1$ rad; $\alpha_r = 0.05$ rad; $\Omega = 30$ rad/sec.

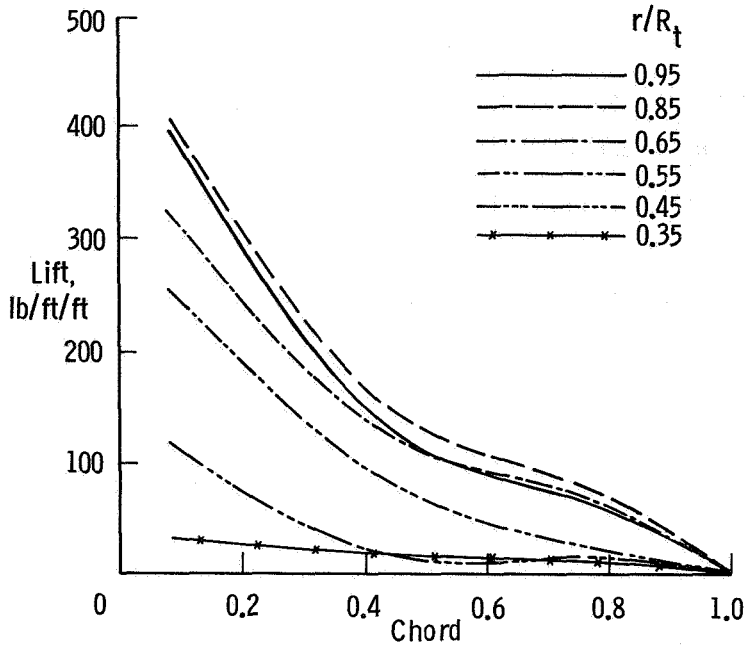

Figure 3. Chordwise pressure distribution for several spanwise locations. $\psi = 90°$; incompressible; $\mu = 0.17$; $\theta_B = 0.1$ rad; $\alpha_r = 0.05$ rad; $\Omega = 30$ rad/sec.

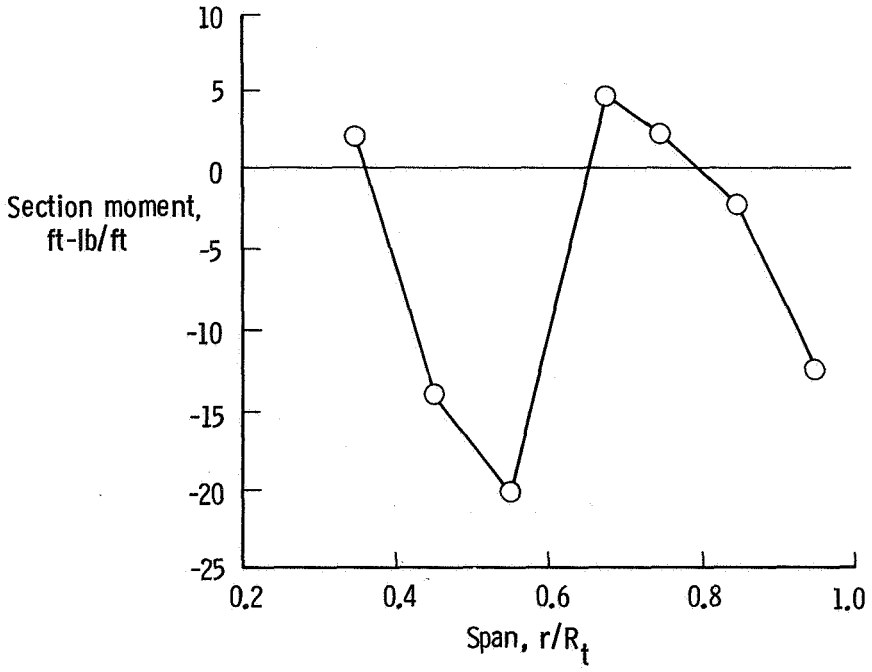

Figure 4. Spanwise section moment distribution about 1/4 C. Positive nose down; $\psi = 90°$; incompressible; $\mu = 0.17$; $\theta_B = 0.1$ rad; $\alpha_r = 0.05$ rad; $\Omega = 30$ rad/sec.

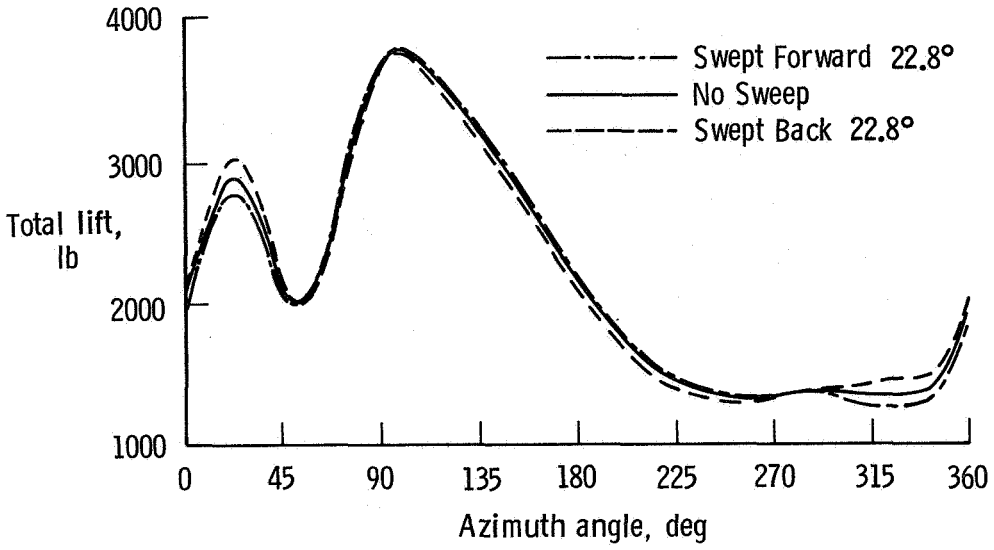

Figure 5. Comparison of lift on a swept-back zero-sweep and swept-forward blade. Incompressible; $\mu = 0.17$; $\theta_B = 0.1$ rad; $\alpha_r = 0.05$ rad; $\Omega = 30$ rad/sec.

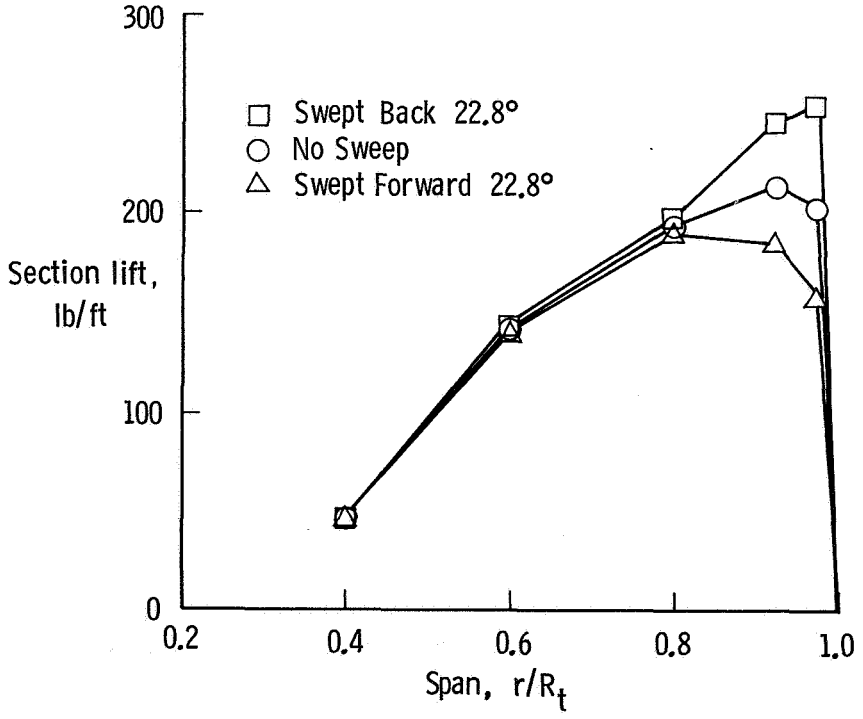

Figure 6. Spanwise section lift distribution for swept-tip configurations. $\psi = 0°$; incompressible; $\mu = 0.17$; $\theta_B = 0.1$ rad; $\alpha_r = 0.05$ rad; $\Omega = 30$ rad/sec.

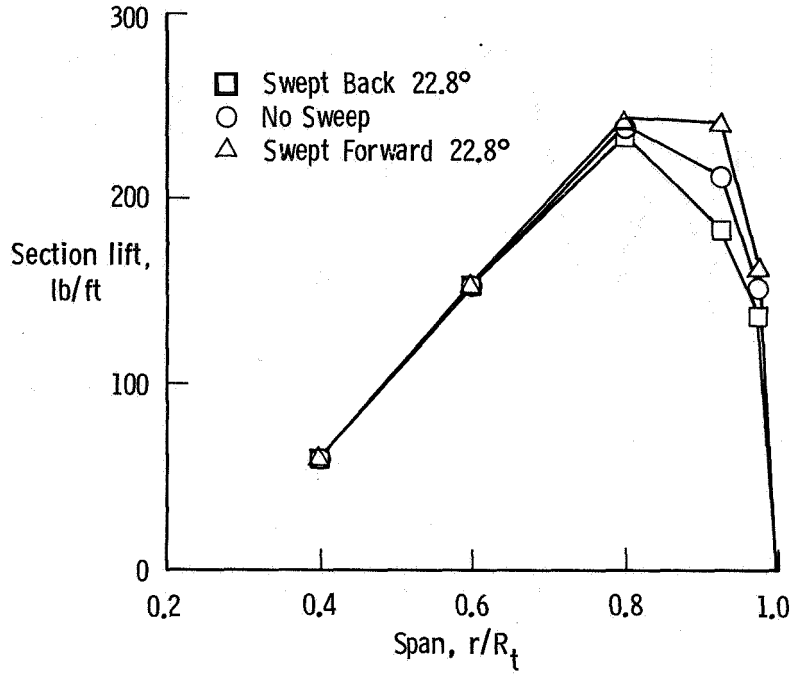

Figure 7. Spanwise section lift distribution for swept-tip configurations. $\psi = 180°$; incompressible; $\mu = 0.17$; $\theta_B = 0.1$ rad; $\alpha_r = 0.05$ rad; $\Omega = 30$ rad/sec.

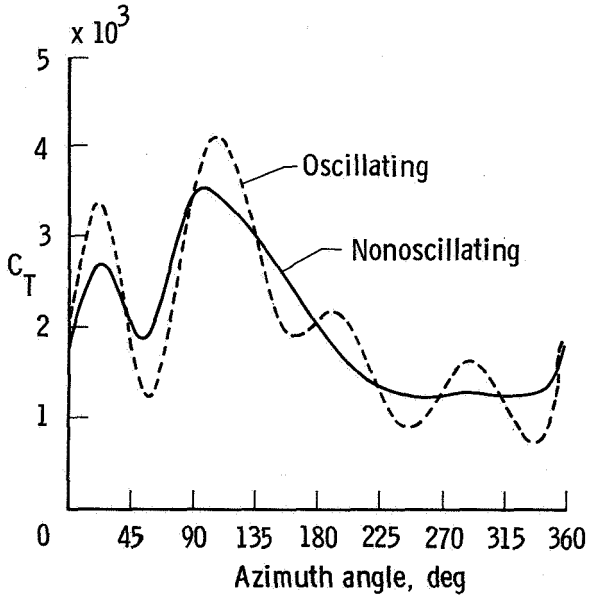

Figure 8. Comparison of lift on a rotor blade oscillating in pitch at 4 per revolution with lift on a nonoscillating blade. Incompressible; $\mu = 0.17$; $\theta_B = 0.1$ rad; $\alpha_r = 0.05$ rad; $\Omega = 30$ rad/sec.

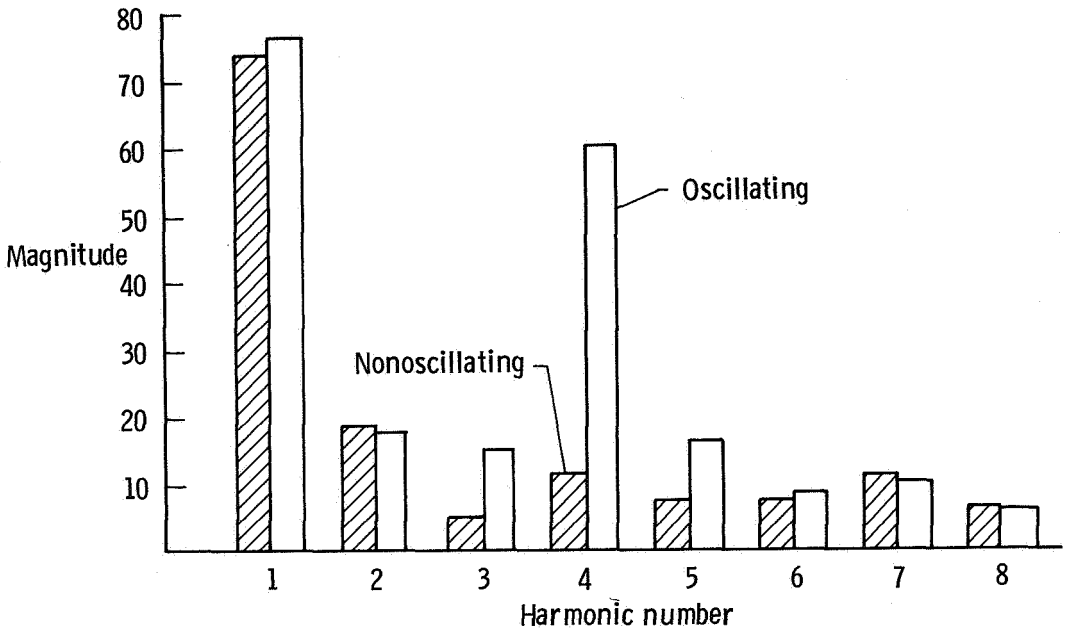

Figure 9. Harmonic content for nonoscillating and oscillating cases. $r/R_t = 0.95$; incompressible; $\mu = 0.17$; $\theta_B = 0.1$ rad; $\alpha_r = 0.05$ rad; $\Omega = 30$ rad/sec.

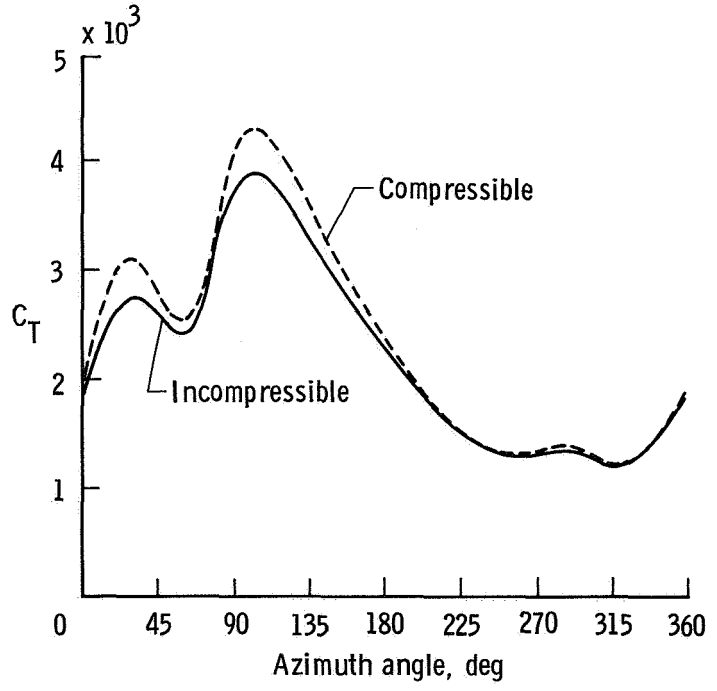

Figure 10. Incompressible and compressible lift for one-bladed rotor. $\mu = 0.17$; $\theta_B = 0.1$ rad; $\alpha_r = 0.05$ rad; $M_{\text{tip}} = 0.54$.

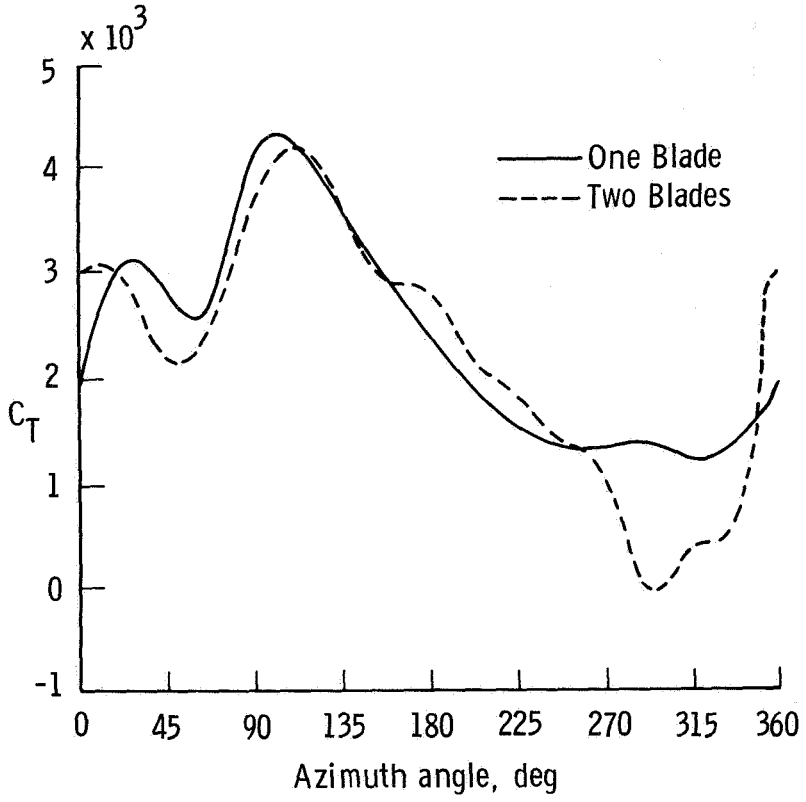

Figure 11. Lift on two-bladed and one-bladed rotor plotted against azimuth angle. Compressible; $\mu = 0.17$; $\theta_B = 0.1$ rad; $\alpha_r = 0.05$ rad; $M_{\text{tip}} = 0.54$.

1. Report No.	2. Government Accession No.	3. Recipient's Catalog No.
NASA TP-2503		

4. Title and Subtitle	5. Report Date
Compressible, Unsteady Lifting-Surface Theory for a Helicopter Rotor in Forward Flight	December 1985
	6. Performing Organization Code: 505-33-43-09
7. Author(s): Harry L. Runyan and Hsiang Tai	8. Performing Organization Report No.: L-15976
9. Performing Organization Name and Address: NASA Langley Research Center, Hampton, VA 23665-5225	10. Work Unit No.
	11. Contract or Grant No.
12. Sponsoring Agency Name and Address: National Aeronautics and Space Administration, Washington, DC 20546-0001	13. Type of Report and Period Covered: Technical Paper
	14. Sponsoring Agency Code

15. Supplementary Notes

16. Abstract

A lifting-surface theory has been developed for a helicopter rotor in forward flight for compressible and incompressible flow. The method utilizes the concept of the linearized acceleration potential and makes use of the doublet lattice procedure. Calculations demonstrating the application of the method are given in terms of the lift distribution on a one-bladed rotor, a two-bladed rotor, and a rotor with swept-forward and swept-back tips. Also, the lift on a rotor vibrating in a pitching mode at 4 per revolution is given. Compressibility effects and interference effects for a two-bladed rotor are discussed.

17. Key Words (Suggested by Authors(s))	18. Distribution Statement
Helicopter Rotor Lifting surface Unsteady flow Compressible flow Acceleration potential	Unclassified—Unlimited Subject Category 02

19. Security Classif.(of this report)	20. Security Classif.(of this page)	21. No. of Pages	22. Price
Unclassified	Unclassified	19	A02

For sale by the National Technical Information Service, Springfield, Virginia 22161

NASA-Langley, 1985